N. Fedorczak, P. Monier-Garbet, T. Pütterich, S. Brezinsek, P. Devynck,
R. Dumont, M. Goniche, E. Joffrin, E. Lerche B. Lipschultz, E. de la Luna,
G. Maddison, C. Maggi, G. Matthews, I. Nunes, F. Rimini, E.R. Solano,
P. Tamain, M. Tsalas, P. de Vries and JET-EFDA contributors

Tungsten Transport and Sources Control in JET ITER-Like Wall H-mode Plasmas

Tungsten Transport and Sources Control in JET ITER-Like Wall H-mode Plasmas

N. Fedorczak[1], P. Monier-Garbet[1], T. Pütterich[8], S. Brezinsek[2], P. Devynck[1],
R. Dumont[1], M. Goniche[1], E. Joffrin[1], E. Lerche[3,4], B. Lipschultz[5], E. de la Luna[6],
G. Maddison[7], C. Maggi[8], G. Matthews[7], I. Nunes[9], F. Rimini[7], E.R. Solano[6],
P. Tamain[1], M. Tsalas[10], P. de Vries[11] and JET-EFDA contributors*

JET-EFDA, Culham Science Centre, OX14 3DB, Abingdon, UK

[1]*CEA, IRFM, F-13108 Saint-Paul-Lez-Durance, France*
[2]*Institute of Energy and Climate Research, Forschungszentrum Jülich, Assoc EURATOM-FZJ, Jülich, Germany*
[3]*Association EURATOM-Belgian State, LPP-ERM-KMS, TEC partner, Brussels, Belgium*
[4]*EURATOM-CCFE Fusion Association, Culham Science Centre, OX14 3DB, Abingdon, OXON, UK*
[5]*York Plasma Institute, University of York, Heslington, York, YO10 5DD UK*
[6]*Laboratorio Nacional de Fusin, Asociacin EURATOM/CIEMAT, 28040 Madrid, Spain*
[7]*Culham Centre for Fusion Energy, EURATOM-CCFE Association, Abingdon, UK*
[8]*MPI fur Plasmaphysik, EURATOM Association, Boltzmannstrasse 2, 85748 Garching, Germany*
[9]*Istituto de plasmas e fusao nuclear, Lisboa, Portugal*
[10]*Association EURATOM-Hellenic Republic, NCSR Demokritos 153 10, Attica, Greece*
[1]*ITER Organization, Route de Vinon sur Verdon, 13115 Saint Paul Lez Durance, France*
* See annex of F. Romanelli et al, "Overview of JET Results",
(24th IAEA Fusion Energy Conference, San Diego, USA (2012)).

ABSTRACT

A set of H-mode discharges performed in JET ITER like wall is investigated with respect to control capabilities on tungsten sources and transport. In attached divertor regimes, increasing fuelling by gas puff increases both divertor plasma collisionality and ELM frequency, resulting in a significant decrease of core plasma radiation. Both pedestal flushing by ELMs and divertor screening (including redeposition) are possibly on tasks. For specific scenarios, vertical kicks can be employed to increase the ELM frequency, which results in slightly lower core radiation. The application of central ion cyclotron minority heating is efficient to increase the core electron temperature gradient and flatten electron density prole, which results in a significantly lower central impurity peaking. Beryllium evaporation in the main chamber did not reduce the local divertor tungsten source whereas core radiation was reduced by approximately 50%.

1. INTRODUCTION

Tungsten (W) as divertor material offers both relevant armor life time [1] and minimum fuel retention [2] for a reactor-grade tokamak operation, as tested in JET with the new ITER-like wall (ILW) [3]. The operational drawbacks are possible wall melting [4] under extreme heat load, and pollution of the conned plasma by radiating high-Z ions. As experienced in ASDEX-Upgrade (AUG) [5; 6] and now in JET [7], this pollution must be controlled to avoid radiation levels incompatible with high confinement (H-mode) operation, generally at a cost of reduced confinement performances [7]. For instance, AUG H-modes are generally performed at non zeros gas puff in the divertor to ensure high edge localized modes (ELMs) frequency and to reduce divertor electron temperature (T_e) and thereby the W source [5]. These ELMs prevent tungsten to enter the conned region, but also increase the energy and particle losses. Central electron heating is also generally applied to repulse tungsten ions from plasma center. Finally, boronizations are performed to reduce the tungsten source from the wall. In this contribution we focus on techniques tested in JET-ILW to control tungsten sources and transport in H-mode attached divertor plasmas. In the first part, we expose some physics involved in plasma pollution by tungsten ions, linked to the interpretation of experimental data and discharge behavior. In a second part we present the experimental setup and some aspects of data interpretation concerning tungsten density and source estimate. In the third part we discuss the experimental observations. First, the influence of divertor gas puff on discharge pollution is investigated in the scope of ELMs flushing and divertor screening. The beneficial impact of artificially increased ELMs frequency by magnetic perturbation is discussed. Then, the beneficial impact of main chamber beryllium evaporation is investigated. Finally, core pollution control with central ion cyclotron resonance heating is addressed.

2. PHYSICS OF TUNGSTEN SOURCE AND TRANSPORT

Tungsten source originates from physical sputtering of tungsten surfaces by impacting ions. Thermal deuterium ions have a small contribution and light impurities generally dominate: residual

carbon, boron and oxygen in the case of ASDEX Upgrade [8], beryllium in the case of JET-ILW [9]. Energetic deuterium ions originating from ELMs or neutral beam injection (NBI) can however significantly contribute to tungsten source [10], or ions accelerated in reciftied sheath potential in the surrounding of ICRH antennae [11].Once sputtered, tungsten atoms ionize on a millimeter range by collision with thermal electrons. If ionization occurs within the magnetic pre-sheath of the local surface (case for most erosion areas except maybe for antennae guard limiters), recent experiments [9] and numerical investigations [12] suggest that a large fraction (ordering 100%) of these tungsten ions are redeposited on the surface without leaving the magnetic pre-sheath. The small fraction (ordering 1%) of escaping ions spreads along field lines via thermodynamical forces (proportional to parallel temperature gradient) but against friction with parallel main ion ow [13]. Turbulent diffusion [14] transports the ions across flux surfaces up to the separatrix, typically on a millisecond time scale [15]. For source areas located above X-point (main chamber or divertor baffles), transport up to the separatrix is faciliated by the relatively short parallel connection length to the main SOL in contact with the separatrix. On the contrary, divertor sources are better screened due to long parallel connection around X-point, accentuated by the divertor collisionality [16].

Once across the separatrix, neoclassical transport is considered to dominate the inward transport of heavy impurity across the pedestal region [14]. Quite generally, the inward pinch increases with density gradient and decreases with temperature gradient. For JET pedestal parameters, the pinch is generally inward through the pedestal and the conned region. Quasi-periodic pedestal relaxation associated to ELMs flush out a significant fraction of ions from the pedestal to the SOL [17, 18]. By this mechanism, increasing ELM frequency leads to a better pedestal screening of the neoclassical inward pinch [5, 14]. The relevant parameter there may be linked to the period between ELMs with respect to the pinch time to cross the pedestal width. On the other hand, the excess of particle and energy deposited into the SOL volume by an ELM induces a strong modification of the SOL tungsten flux from the surfaces to the separatrix: (1) the neutral W source is increased [19, 9] far above the inter-ELM level; (2) magnetic pre-sheath redeposition may however increase [12]; (3) screening along field line may be reduced [16].

In the conned plasma volume inside the pedestal, tungsten ions are strongly ionized and radiate in the XUV range [20]. Photon emissivity is extremely strong in the electron temperature range 1–3keV, which significantly increases the level of radiated power from inside the separatrix compared to scenarios without tungsten [7]. First, kinetic losses crossing the separatrix are reduced, leading to possible modification of tungsten source and transport in the SOL. It would also tend to decrease the type-I ELM frequency, impacting also the tungsten transport at the edge. Eventually, the power through separatrix can fall below the high to low (L) confinement mode power threshold and the plasma transits into L-mode. Second, radiation can cause local energy unbalance which results in the local cooling down of thermal electrons. This happens preferentially at the very center of the plasma where tungsten ions tend to cumulate [5, 20]. Once the energy unbalance starts, electron temperature prole flattens, increasing the neoclassical inward pinch, in turns accentuating the

2

particle accumulation at the very center. This vicious cycle leads to an uncontrolled situation eventually ending in a disruption, but which can be counter-acted with sufficient amount of local electron heating [5]. In ASDEX Upgrade, ECRH and ICRH heating are commonly used for this task [11]. The counterpart of ICRH application is a global increase of core radiation, probably due to an enhanced main chamber tungsten source caused by ICRH antennae polarization. Moreover, MHD activity like saw-teeth also impacts the tungsten transport in core plasmas [21, 22, 23]. A quasi periodic expulsion of particle from the plasma center competes with impurity inward pinch the same manner as ELMs act in the pedestal.

3. EXPERIMENTAL SETUP

3.1. PLASMA SCENARIOS

The investigation of tungsten control by application of ICRH central heating and ELM pacing with kicks, in a relevant ITER baseline scenario ($q_{95} \approx 3$) has been performed in two types of scenarios. Central ICRH electron heating at $f_{ICF} = 42$MHz with hydrogen minority ions requires a magnetic field at plasma center $B_T = 2.7$T and so $I_P = 2.5$MA, but ELM triggering by kicks has a higher reliability at lower plasma current [24], which imposes a lower magnetic field at xed safety factor. ELM pacing by kicks is tested on a rst scenario at $I_P = 2.0$MA, $B_T = 2.1$T on magnetic axis, low plasma triangularity $\delta_l = 0.36$, $\delta_u = 0.19$, pure NBI heating $P_{NBI} = 12$MW resulting in a moderate normalized plasma pressure $\beta_p = 0.5$–0.7. The outer strike point is static on the bulk tungsten tile (tile 5) and the inner strike point on the vertical target (see Fig.1a). Gas fuelling is performed in the divertor volume, either in the private flux region (GIM11), or outside the outer strike point (GIM9). ELM frequency is either modified by a shot to shot scan of the fuelling rate during the H-mode phase, in the range $\Gamma_e = 0$ to 10^{22}s^{-1}, or by application of kicks of higher frequency than the natural ELM frequency obtained at a given fuelling rate.

In order to perform ion cyclotron hydrogen minority heating, a second scenario was considered at $I_P = 2.5$MA, $B_T = 2.7$T, $P_{NBI} = 12$–18MW and $P_{ICRH} = 0$–5MW. The minority hydrogen concentration is about $c_H \approx 7\%$, allowing central electron heating for $P_{ICRH} \geq 3$MW. Plasma shape is identical as in the previous scenario, exept the outer strike point which is radially swept along the bulk tungsten tile (by about 5cm at 5Hz) in order to spread the larger heat load. Besides central heating, the gas fuelling rate was also scaned to control the ELM frequency and core radiation. In order to optimize the coupling resistance of ICRH antennae, the gas fuelling was performed by an arrangement of main chamber nozzles instead of divertor nozzles [25]. This scenario was finally selected to test the consequence of a beryllium evaporation in the main plasma chamber by comparing two series of pulses with identical settings performed before/after the evaporation.

3.2. DIAGNOSTICS

Tungsten source at the surface of divertor target is monitored by visible spectroscopy [9] with a spatial resolution of about $\Delta R = 15$mm. The W^0 line at 400.9nm is fitted out of the background,

with a time resolution of about 40ms. This photon flux can be interpreted in term of particle flux via a collisional-radiative model [26]. The number of ionization per emitted photon, written $\frac{S}{SXB}$, is a function of electron temperature [9], so that visible spectroscopy coupled to, for instance, Langmuir probe measurement of T_e, can yield a quantitative estimate of the flux of tungsten atoms produced at the target. A prole of photon flux is shown in Fig.1c. The photon flux along the outer divertor tile exhibits a pattern relatively close to the saturation ion flux collected by an array of Langmuir probes (also shown in Fig.1c). To be fully consistent and evaluate the total number of tungsten atoms leaving the surface, the local photon flux should be multiplied by a local $\frac{S}{SXB}$ (T_e) value, then integrated over the divertor surface. The time evolution during ELMs should be treated as well. Unfortunately, interpretation of probe measurements with ELM is subject to large errors and generally the time resolution of spectroscopy does not allow the clear distinction of inter-ELM versus intra-ELM tungsten flux. Current investigations suggest that, in the scenarios investigated here (non detached divertor), inter and intra ELMs contributions to the W source are of equal amplitude [27]. For simplicity, signals are averaged over 1 second and we consider a constant and uniform value $\frac{S}{SXB}$ = 30, used across the series of pulses. This yields an effective number of emitted tungsten atoms from the bulk tungsten tile, assumed representative of the tungsten flux emitted by the divertor. Note also that W-components are present in the main chamber of JET-ILW which are not monitored by spectroscopy: the outer and inner divertor baffle made of tungsten coating, and some recessed areas within the beryllium main chamber [28].

The transport of ionized tungsten from the divertor surface up to the separatrix cannot be directly measured in JET. On the other hand, the ionized tungsten density in the conned region can be estimated from soft X-ray (SXR) measurements [29]. After a tomographic reconstruction of the SXR radiation pattern, a bremsstrahlung component is subtracted (see Fig.1a), and de convoluted into a tungsten density (considered as the only radiator), assuming electron temperature and density uniform on flux surfaces. This tungsten density map is then integrated over the conned plasma volume, with an extrapolation for flux surfaces where T_e < 1.5keV, to yield the total number of tungsten atoms in the conned region N_W. For comparison, we also constructed a proxy for this quantity from the total radiated power P_{RAD} (from the bulk plasma) measured by bolometers, assuming $P_{RAD} \approx N_W\, n_e L_W^{eff}$ where ne is a vertical line averaged electron density measured by interfero-polarimetry and L_W^{eff} is an effective cooling factor for tungsten ions in coronal equilibrium [20]. In the following, we use $L_W^{eff} = 5.10^{-31}\,Wm^3$ which stands for the maximum of the cooling factor reached at $T_e = 1.5keV$. As seen in Fig.1c), proxy and SXR estimates of the tungsten amount are in relatively good agreement over one decade, within 50% error. In the following, the bolometry estimate of the tungsten content is considered, both for its simple expression and its direct proportionality with core radiation.

4. EXPERIMENTAL RESULTS
4.1. GAS FUELLING
Increasing the fuelling rate is commonly used in AUG to increase ELM frequency in order to mitigate

the conned plasma radiation caused by tungsten [5]. As shown in Fig.2 and previously reported [7], a finite fuelling rate is mandatory in JET-ILW to avoid H-mode collapse by radiation. In the scenario investigated here, a large divertor fuelling rate ($\Gamma_e \approx 15{\times}10^{21}\mathrm{s}^{-1}$) is applied over typically 1 second prior to H-mode formation, before being reduced to the desired value. By this means, early H-mode ELM free phases are avoided. At medium divertor fuelling rate $\Gamma_e \approx 4.5{\times}10^{21}\mathrm{s}^{-1}$, ELM frequency is about $f_{ELM} = 20\mathrm{Hz}$ and the radiated power is stable around 2MW throughout the H-mode phase. At $\Gamma_e \approx 1{\times}10^{21}\mathrm{s}^{-1}$, ELM frequency falls to about 10Hz, and the radiated power increases to 5MW with no sign of collapse after 4s of H-mode. When fuelling is switched o during H-mode (except from NBI), ELM frequency drops to a few Hz and radiated power increases to about 9MW in the first seconds of the H-mode phase. Note that the fast increase of core radiation is associated to an ELM free phase (around t = 9.5s) lasting less than 0.5s. Concomitant is an increase of the density prole peaking (from pedestal top to core), resulting in a further increase of the radiated power (starting at 10.5s in Fig.2). Although the line averaged density is constant throughout the H-mode plateau, pedestal density continuously falls with low frequency bursts of compounds ELMs, and central density rises, probably due to core cooling. After approximately 2sec of H-mode, the plasma falls back into L-mode. The impact of divertor fuelling rate on H-mode behavior is summarized in Fig.3 where the trends across series of pulses are illustrated. Instead of fuelling rate, the ion recycling flux on the outer divertor target is considered as a marker of divertor regime, (it is collinear with the fuelling rate but with dierent proportionality depending on the injector location). Across the fuelling scan, this ion flux varies by a factor of 5 still below detachment, while core electron density from pedestal to core only varies by less than 20%. As noted previously [7] and shown in Fig.3c, increasing the divertor recycling decreases the tungsten source $\Gamma_W \propto \Gamma_i^{-0.5(-0.8)}$ for $B_T = 2.1\mathrm{T}$ ($B_T = 2.7\mathrm{T}$) scenario. This behavior indicates that the effective sputtering rate decreases by an order of magnitude from $Y_W \approx 2.10^{-3}$ to 2.10^{-4} when recycling is increased. The two possible reasons are (1) a change of the impurity content in the divertor, especially of beryllium ions, (2) a reduction of ion impact energy by dillution, which strongly lowers the sputtering yield. We can verify that the power across the separatrix devided by the ion recycling rate, yielding an effective impact energy, falls by a factor of 2.5 across the fuelling scan. Lower impact energy also suggests lower electron temperature in the divertor, suggesting a decreasing S/XB value with increased recycling. Therefore the decrease of the tungsten source with recyling rate is possibly stronger than expected. Assuming that about half the outpout power reaches the outer strike point with a sheath energy transmission of about $\gamma = 10$, the electron temperature at the divertor surface varies roughly from $T_e = 65\mathrm{eV}$ to $T_e = 25\mathrm{eV}$ across the fuelling scan. Correcting the S/XB dependence with this temperature yields a tungsten source varying with recycling as $\Gamma_W \propto \Gamma_i^{-0.6(-1.0)}$ for $B_T = 2.1\mathrm{T}$ ($B_T = 2.7\mathrm{T}$), thus close to the trends obtained with constant S/XB value. Note that for $B_T = 2.1\mathrm{T}$ pulses, the tungsgten source is higher and show more scatter than for $B_T = 2.1\mathrm{T}$ pulses probably because of dierent heating schemes and larger injected power, although SOL losses are of the same order (Fig.3d).

Second, the total tungsten content is also decreasing with increased recycling rate

$N_W \propto \Gamma_i^{-1.1(-1.5)}$ for $B_T = 2.1T$ ($B_T = 2.7T$). It cannot be solely attributed to variation of the source, because the ratio of both $\tau_W = \frac{N_W}{\tau_W}$, either called effective confinement time [14, 30] or penetration factor [31], is also decreasing with divertor recycling $\tau_W \propto \Gamma_i^{-0.6(-0.7)}$. Assuming that the dominant tungsten source is the outer divertor, it means that tungsten transport from divertor to the conned region is globally impacted by edge fuelling: divertor screening and/or pedestal transport. As stated above, ELM frequency increases with recycling $f_{ELM} \propto \Gamma_i^{1.3(1.5)}$ for $B_T = 2.1T$ ($B_T = 2.7T$). Combining the trends, we nd that tungsten penetration factor decreases with ELM frequency, with the same trend for both scenarios $\tau_W \propto f_{ELM}^{-0.45}$ (see Fig.4). In [14], a model of tungsten flushing by ELMs is detailed, proposing an inverse proportionality between W confinement time and ELM frequency $\tau_W \propto f_{ELM}^{-1.1}$, although divertor screening is not included in the model.

Fuelling may directly increase the ELM frequency, leading to an increased W flushing at pedestal. On the other hand, we can also propose an alternative interpretation. We see from Fig.3a,b that higher ELM frequency and lower core radiation level are correlated. In facts, ELMs frequency linearly increases with power through separatrix above a given threshold (Fig.3d), which is a typical behavior of type-I ELMs. Thus, it could also be that ELM frequency is not directly controlled by fuelling in these set of experiments, but rather set by power losses. Thus, tungsten content in the conned region increases non-linearly with the neutral Wdivertor source, because of the pedestal flushing decreasing with increasing core radiation. However, we note again that tungsten divertor screening (including redeposition) may be invoked [13; 9], which should be focused in future analyses of these experiments.

4.2. VERTICAL KICKS

To consolidate the interpretation of the correlation between penetration factor and ELM frequency, a subset of pulses from the fuelling scan at $B_T = 2.1T$ have been identically repeated, with vertical kicks starting at H-mode formation. It should be noted that application of kicks did not change the divertor recycling level at given fuelling, nor the pedestal proles. For relatively high natural ELM frequency ($f_{ELM} \geq 20Hz$), vertical kicks have a good probability ($p_{trig} \approx 80\%$) to trigger ELMs at a frequency 50% above the natural one. As shown in Fig.4, W obtained with these kicks is similar to the penetration factor obtained at the same natural ELM frequency with higher recycling. This could confirm the control of tungsten penetration with ELM frequency. That said, it is observed in a domain where ELM frequency is high and tungsten radiation is already low. At lower natural ELM frequency $f_{ELM} \approx 10Hz$ obtained at lower fuelling/recycling, the application of 20Hz kicks was unsuccessful to trigger ELMs ($p_{trig} \approx 60\%$) even at the beginning of H-mode. Plasma radiation reached significantly higher level than without kicks, in two consecutive pulses. The core radiation leads to a drop of pedesetal temperature (from about 700eV to less than 500eV in less than 1 sec), further preventing the kicks to trigger ELMs [24] at higher pedestal collisionality. The reason for increased radiation is presently unknown, but the mechanism may involve low divertor screening at low fuelling and non monitored tungsten sources induced by kicks (possibly dusts).

4.3. BERYLLIUM EVAPORATION

So far we have investigated the tungsten transport from the outer divertor source. In order to reduce the apparent tungsten areas facing the plasma, a beryllium evaporation was applied in the main chamber. A set of pulses were repeated after the evaporation with identical control parameters (fuelling, heating, etc). An illustration is shown in Fig.5a. Beryllium evaporation leads to a lower plasma density (20%) for similar fuelling, probably due a higher fuel trapping in beryllium layers. As shown in Fig.5b, the effective core tungsten content is about 40% lower than reference in the rst H-mode following the evaporation, but increases toward the reference value across successive H-mode phases with a time scale in the order of 10 seconds. Interestingly, the source of tungsten from the divertor is slightly higher after evaporation probably due to a higher beryllium ion concentration in the divertor. It suggests that evaporation did not efficiently cover the divertor tungsten tiles. Also, the evaporation did not modify the ELM frequency dependence with power losses (shown in Fig.3d). From this alone, we cannot explain why beryllium evaporation leads to a higher ELM frequency and a lower amount of tungsten ions in the core. One possibility is that main chamber (divertor excluded) tungsten layers where effectively covered by beryllium, and that the associated tungsten source is reduced after evaporation. In AUG, these sources dominate the plasma pollution with respect to divertor sources [19] due to poor screening. In JET however, main chamber tungsten areas are very limited, but could anyhow participate in the plasma pollution. This point should be further investigated, because it suggest as in AUG that divertor source is not the relevant quantity controlling the core pollution. This conclusion needs to be addressed with specific spectroscopic measurements in the JET-ILW main chamber.

4.4. CENTRAL ICRH HEATING

Now we investigate tungsten transport through the core. As mentioned previously (Fig.2), a large increase of core radiation is correlated with an increase of electron density peaking [20]. In facts, the radiation peaking is increasing as well. To test the effect of electron prole on impurity peaking, ion cyclotron hydrogen minority heating is applied. A set of pulses is selected, with similar fuelling rate $\Gamma_e \approx 5.5 \times 10^{21} s^{-1}$, similar heating power $P_{TOT} \approx 17 MW$ but varying ICRH fraction (0 to 25%). As shown in Fig.6a, central ICRH heating increases the electron temperature gradient (ETG) by about 40% with 25% of heating provided by ICRH, whereas electron density gradient decreases by more than 50%. Both effects are supposed to either decrease the inward pinch or increase outward impurity ow [32], which is indeed suggested by the strong decrease (by a factor of 3) of central radiation peaking shown in Fig.6b. This peaking is simply calculated from the ratio of two channels of an horizontal bolometer, one passing by the plasma center ($\rho = 0$), one passing above at $\rho = 0.3$ (see Fig.1a). A concomitant effect of ICRH is a global increase of core radation (from 5 to 10MW with 4MW of ICRH), although outer divertor source is apparently not impacted by ICRH. This may suggest, as in AUG, that ICRH induces an increase of main chamber tungsen sources at location magnetically connected to the antennae. But it could also be a consequence of the release of

Nickel [33] which composes the Faraday screen of the antennae. The (peaking) attening of electron (temperature) density prole with ICRH offers a convenient control actuator to avoid central tungsten accumulation, as demonstrated in AUG [34].

CONCLUSION AND DISCUSSION

So far, standard H-mode operation in JET-ILWis conducted with substantial divertor gas fuelling to maintain low radiation level, but at the drawback of reduced energy confinement [7]. This is probably caused by a lower pedestal temperature at higher fuelling [35]. In non detached divertor conditions, control of core radiation by fuelling can be attributed to three processes: (1) a lower tungsten source originated from the outer divertor plate, (2) a higher screening efficiency of the divertor volume, (3) a better pedestal flushing caused by increased ELM frequency. The application of vertical kicks to increase ELM frequency at given fuelling suggest that a dominant mechanism is flushing at relatively high ELM frequency; although the principle was not conclusive at low fuelling, for which flushing control would have been of primary interest. An alternative to vertical kicks is the use of deuterium pellets to trigger ELMS, efficient at higher plasma current. Current results however suggest that the ELM frequency obtained with pellet is relatively close to the one obtained with fuelling alone, at the rate imposed by pellets. In terms of control, it is however not yet clear if fuelling is directly impacting ELM frequency. In the set of experiments conducted here, with non-detached outer divertor, it seems that ELMs are of type-I suggested by the increase of their frequency with the kinetic power losses across separatrix, higher at low radiation level. Fuelling controls the tungsten source via dilution of ion energy, and probably its screening and redeposition in the divertor volume. Thus at increased fuelling, a lower amount of tungsten can reach the separatrix, which globally lowers the core radiation level. Therefore, ELM frequency increases and further reduces the core radiation, whereas the increased power crossing the separatrix both in between and during ELMs may impact the tungsten source. These nonlinear mechanisms linking core radiation and edge sputtering are of primary importance to understand how to efficiently control the level of core radiation with simple actuators like divertor fuelling. It has also to be mentioned that the outer divertor may not be the relevant source location controlling the plasma pollution in JET-ILW. Discharges conducted after a beryllium evaporation showed no reduction of the outer divertor tungsten source (measured at one toroidal location), whereas core radiation was reduced by 50%. First, ELM frequency is higher just after evaporation, but as suggested by Fig.3d it is probably a consequence of lower core radiation on type-I ELMs. Second, the evaporation is probably non toroidally symmetric, so that a fraction of the tungsten divertor has been covered by a beryllium layer but not at the visible spectroscopy location. Third, the evaporation is more efficient in covering the main chamber elements (including divertor baffle), where originates a tungsten source which may dominate the core plasma pollution. This would be important to measured in future experiments.

Once inside the pedestal, tungsten transport is set by a competition between : (1) neoclassical inward pinch, (2) turbulent diffusion, (3) saw tooth flushing. Central electron heating with ion

cyclotron hydrogen minority scheme can control the radiation peaking at plasma center via a control of both temperature and density gradients. The drawback of ICRH application is an enhanced radiation level, and the necessity to fuel a sufficient amount of gas to couple the wave across SOL plasma. On the other hand, central electron heating provides a higher central temperature than with pure NBI, so that the effective impact of fuelling and radiation on global confinement efficiency could be compensated.

ACKNOWLEDGMENT

REFERENCES

[1]. R.A. Pitts et al. Journal of Nuclear Materials, **438**(0):S48–S56, 2013.

[2]. T. Loarer et al. Journal of Nuclear Materials, **438**(0):S108–S113, 2013.

[3]. G.F. Matthews and EFDA-JET contributors. Physica Scripta, 2011(**T145**):014001, 2011.

[4]. J.W. Coenen et al. Journal of Nuclear Materials, **438**, Supplement(0):S27–S33, 2013.

[5]. A. Kallenbach and ASDEX Upgrade Team. Nuclear Fusion, **49**(4):045007, 2009.

[6]. H. Zohm and et al. Nuclear Fusion, **49**(10):104009, 2009.

[7]. E. Jorin and JET-EFDA Contributors. Nuclear Fusion, **54**(1):013011, 2014.

[8]. Vl.V. Bobkov and ASDEX Upgrade Team. Nuclear Fusion, **50**(3):035004, 2010.

[9]. G.J. van Rooij et al. Journal of Nuclear Materials, **438**, Supplement(0):S42–S47, 2013.

[10]. R. Dux et al. Journal of Nuclear Materials, **363–365**(0):112–116, 2007.

[11]. Vl. Bobkov et al. Journal of Nuclear Materials, **415**(1):S1005–S1008, 2011.

[12]. A.V. Chankin, D P Coster, and R Dux. Plasma Physics and Controlled Fusion, **56**(2):025003, 2014.

[13]. A. Järvinen and JET-EFDA contributors. Physica Scripta, 2011(**T145**):014013, 2011.

[14]. R. Dux and ASDEX Upgrade Team. Nuclear Fusion, **51**(11):119501, 2011.

[15]. M. E. Puiatti and JET-EFDA contributors. Physics of Plasmas, **13**(4):{, 2006.

[16]. A. Jarvinen et al. Journal of Nuclear Materials, **438**(0):S1005–S1009, 2013.

[17]. A. Loarte and EFDA-JET Workprogramme Collaborators. Plasma Physics and Controlled Fusion, **44**(9):1815, 2002.

[18]. H Urano and ASDEX Upgrade Team. Plasma Physics and Controlled Fusion, **45**(9):1571, 2003.

[19]. R. Dux et al. Journal of Nuclear Materials, **390–39**(0):858–863, 2009.

[20]. T. Pütterich and the ASDEX Upgrade Team. Nuclear Fusion, 50(2):025012, 2010.

[21]. M.F.F. Nave, J. Rapp, T. Bolzonella, and contributors to the JET-EFDAWorkprogramme. Nuclear Fusion, **43**(10):1204, 2003.

[22]. T. Pütterich, the ASDEX Upgrade Team, and JET EFDA Contributors. Plasma Physics and Controlled Fusion, **55**(12):124036, 2013.

[23]. T. et al. Nicolas. Physics of Plasmas, 21(1):–, 2014.

[24]. E. de la Luna et al. on JET Proc. 24th IAEA Fusion Energy Conf, 2012.

[25]. E. Lerche et al. this conference, P1-061, 2014.

[26]. K Behringer, H P Summers, B Denne, M Forrest, and M Stamp. Plasma Physics and Controlled Fusion, **31**(14):2059, 1989.

[27]. N. Den Harder and JET-EFDA contributors. This conference, 2014.

[28]. J.W. Coenen et al. This conference, 2014.

[29]. T. Pütterich and the ASDEX Upgrade Team. Plasma Physics and Controlled Fusion, **50**(8):085016, 2008.

[30]. T.T. Pütterich and JET-EFDA Contributors. Proceedings of 24th IAEA Fusion Energy Conference (San Diego, USA), page pp. EXP3.

[31]. B. Lipschultz, D.A. Pappas, B. LaBombard, J.E. Rice, D. Smith, and S.J. Wukitch. Nuclear Fusion, **41**(5):585, 2001.

[32]. M. Valisa and JET-EFDA contributors. Nuclear Fusion, **51**(3):033002, 2011.

[33]. A Czarnecka, F Durodie, and JET-EFDA contributors. Plasma Physics and Controlled Fusion, **54**(7):074013, 2012.

[34]. R. Neu and the ASDEX Upgrade team. Nuclear Fusion, **45**(3):209, 2005.

[35]. M.N.A. Beurskens and JET-EFDA Contributors. Nuclear Fusion, **54**(4):043001, 2014.
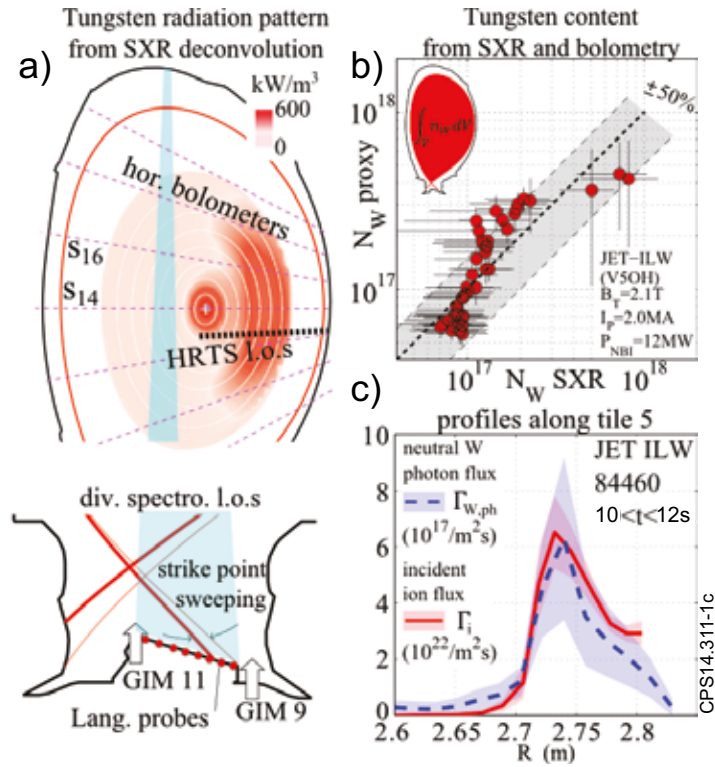
Figure 1: a) JET cross section showing the equilibrium separatrix position, strike points position, and relevant diagnostics geometry. Is also shown a typical tungsten radiation pattern constructed from SXR. b) Tungsten content in the conned volume calculated from SXR compared to its proxy calculated by bolometry, for a series of 10 H-mode pulses. Data are time averaged over 1s windows. c) Profiles along tile 5, of ion flux normal to the surface (Γ_i) and photon flux emitted by neutral tungsten ($\Gamma_{W,ph}$).
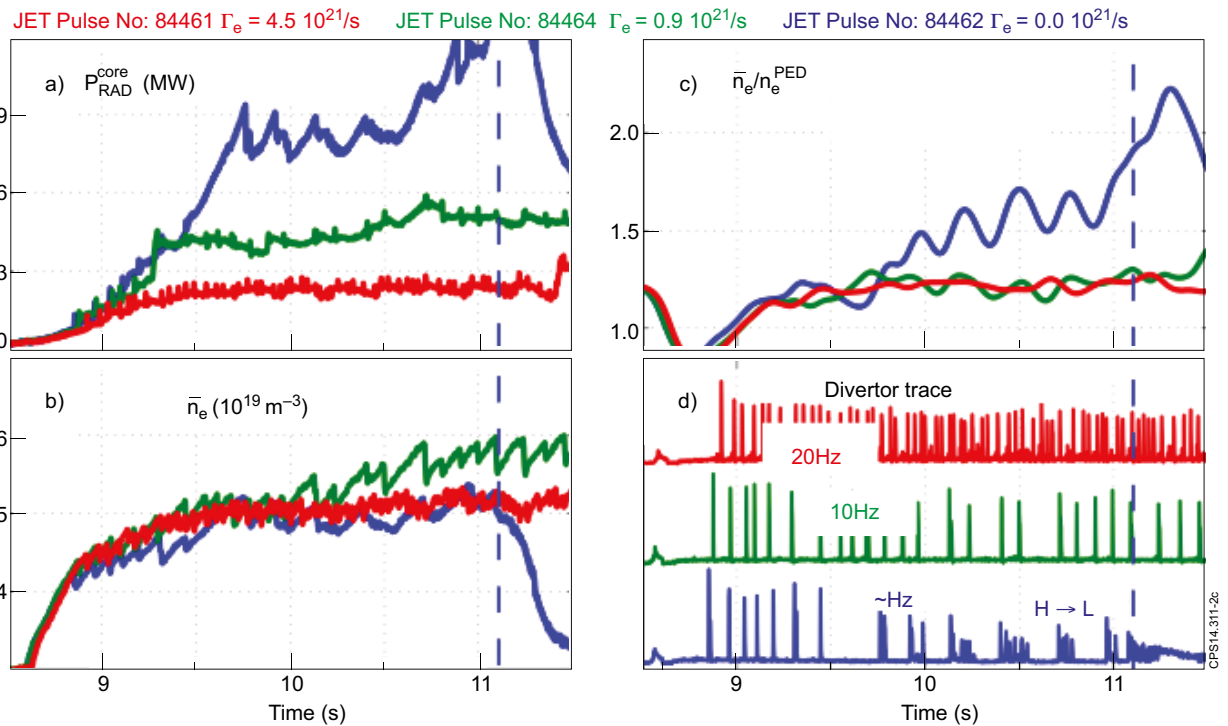
Figure 2: Pulse evolution at dierent H-mode fueling rates, $B_T = 2.1T$, $I_P = 2.0MA$, $P_{NBI} = 2MW$. a) radiated power from conned region, b) line averaged electron density, c) density peaking (line averaged density over pedestal density from HRTS), d) ELM traces from divertor.
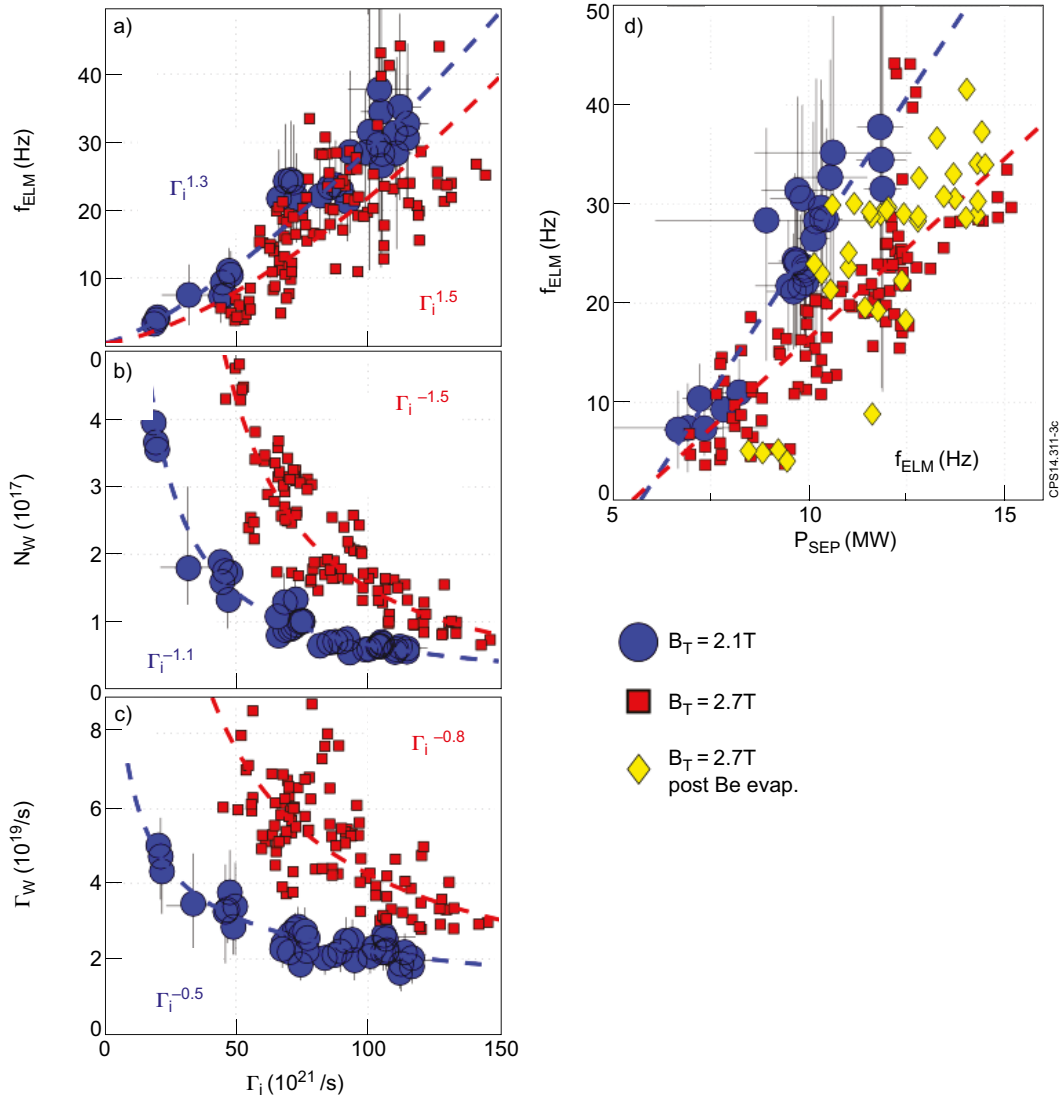
11

Figure 3: Variation of a) ELM frequency, b) total tungsten content, c) outer divertor tungsten source function of outer divertor recycling flux. Dashed curves show the power law trends, with given exponents. d) Variation of ELM frequency versus power through separatrix, dashed curves are linear trends. Each point is a 1s average during H-mode. $B_T = 2.1T$ scenario in blue circles, $B_T = 2.7T$ scenario before (after) Be evaporation in red squares (yellow diamonds)
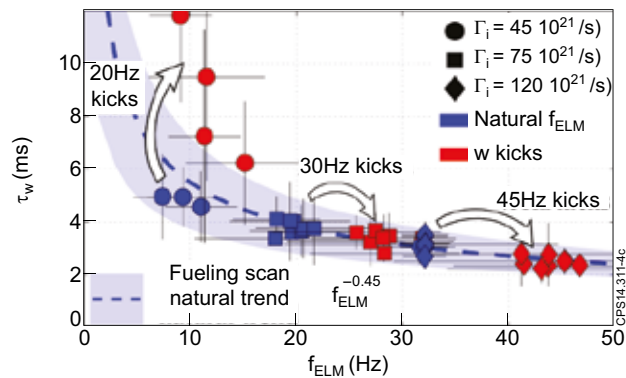

Figure 4: Variation of tungsten penetration factor versus ELM frequency for $B_T = 2.1$ scenario during the fuelling scan (blue trend). Three shot to shot comparisons of the effect of kicks are shown. Each point is a 1s average during H-mode plateau.
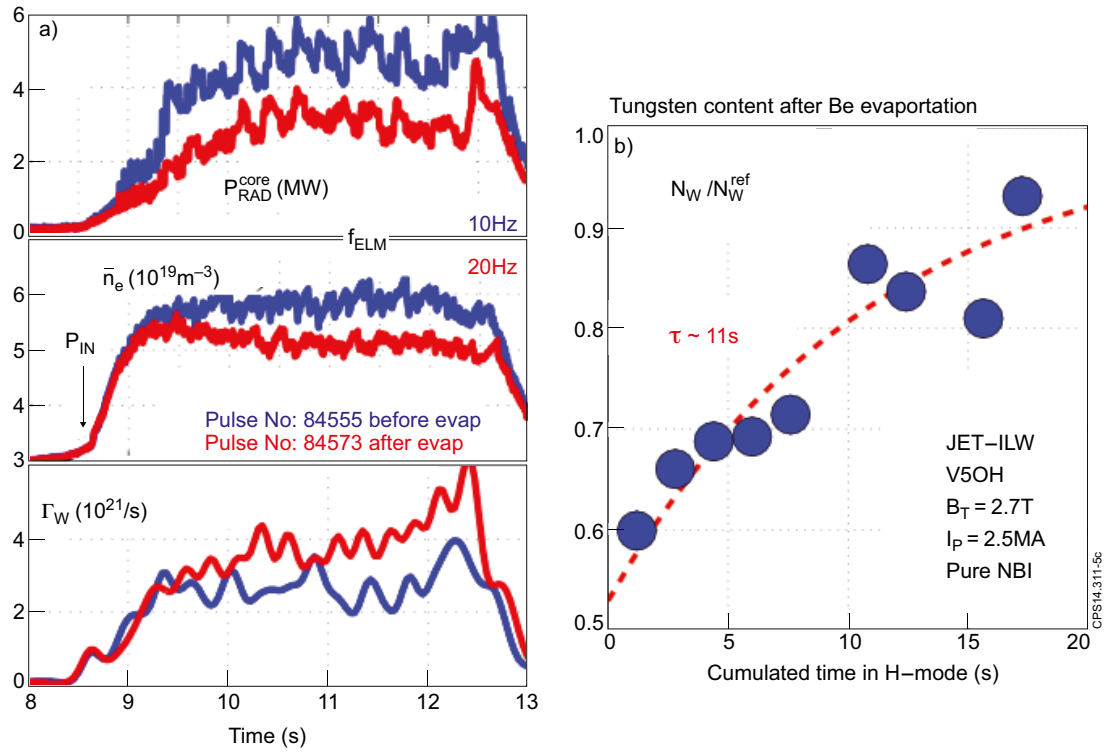
Figure 5: a) Comparison of two NBI heated pulses before (blue) after (red) beryllium evaporation, showing the core radiated power, line averaged electron density, outer divertor tungsten source. b) Evolution of core tungsten content during H-mode from the rst H-mode phase after beryllium evaporation, compared to reference pulses.
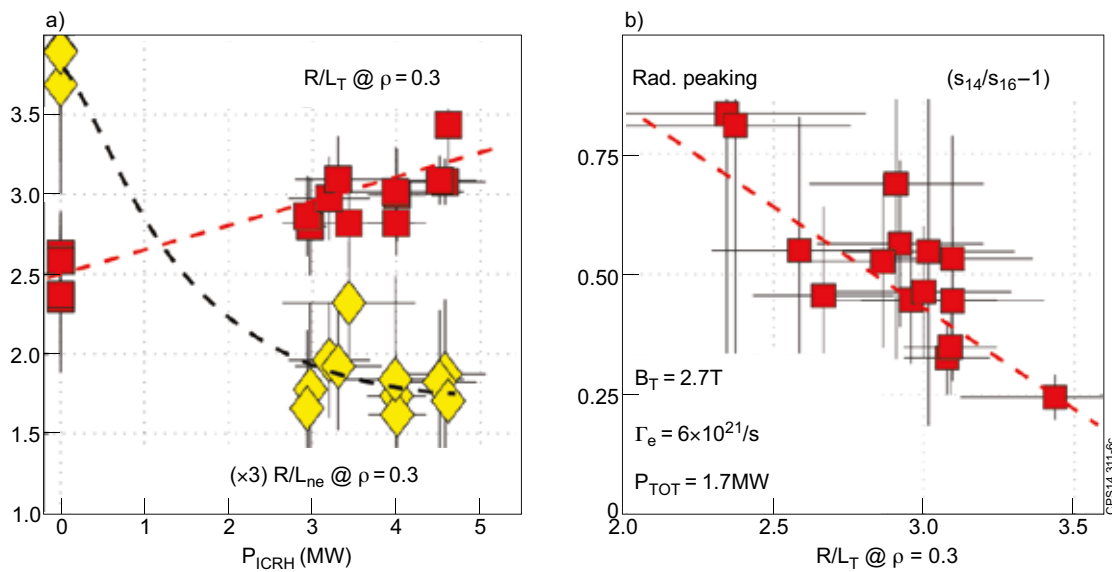

Figure 6: Influence of central ICRH heating on core plasma: a) Core electron temperature (squares) and density (diamonds) gradient versus ICRH power. b) Central radiation peaking versus core temperature gradient. Radiation peaking is evaluated by the ratio of 2 horizontal bolometer channels (Fig.1). Each point is a 2sec average during H-mode in order to smooth saw-tooth induced modulation.